Edwards, T. L., Brandon, M. A., Durand, G., Edwards, N. R., Golledge, N. R., Holden, P. B., Nias, I. J., Payne, A. J., Ritz, C., & Wernecke, A. (2019). Revisiting Antarctic ice loss due to marine ice-cliff instability. *Nature*, *566*, 58-64. https://doi.org/10.1038/s41586-019-0901-4

ARTICLE

Revisiting Antarctic ice loss due to marine ice cliff instability

Tamsin L. Edwards* [a], Mark Brandon [b], Gael Durand [c], Neil R. Edwards [b], Nicholas R. Golledge [d, e], Philip B. Holden [b], Isabel Nias [f], Antony J. Payne [g], Catherine Ritz [c] and Andreas Wernecke [b].

* Corresponding author

a Department of Geography, King's College London

b School of Environment Earth and Ecosystem Sciences, Faculty of Science, Technology, Engineering and Mathematics, Open University, Walton Hall. Milton Keynes, UK

c Univ. Grenoble Alpes, CNRS, IRD, IGE, F-38000 Grenoble, France

d Antarctic Research Centre, Victoria University of Wellington, Wellington 6140, New Zealand

e GNS Science, Avalon, Lower Hutt 5011, New Zealand

f Earth System Science Interdisciplinary Center, 5825 University Research Court, Suite 4001, College Park, Maryland 20740-3823, USA

g Centre for Polar Observation and Modelling, School of Geographical Sciences, University of Bristol, University Road, Bristol BS8 1SS, UK

Predictions for sea-level rise from Antarctica this century range from zero to over one metre. The highest are driven by the controversial 'marine ice cliff instability' (MICI) hypothesis, where coastal ice cliffs rapidly collapse after ice shelves disintegrate from surface and sub-shelf melting caused by global warming. But the MICI mechanism has not been observed in the modern era, and it remains unclear whether or not it is required to reproduce sea-level variations in the geological past. Here we quantify ice sheet modelling uncertainties for the original MICI study and show the probability distributions are skewed towards lower values (most likely value is 45 cm under very high greenhouse gas concentrations). However, MICI is not required to reproduce sea-level changes in the mid-Pliocene, Last Interglacial or 1992-2017, and without it we find the projections agree with previous studies (all 95th percentiles are less than 43 cm). We therefore find previous interpretations of the MICI projections over-estimate sea-level rise this century. The hypothesis is not well constrained: confidence in projections with MICI would require a greater diversity of observationally constrained models of ice shelf vulnerability and ice cliff collapse.

Projections of the Antarctic contribution to global mean sea-level rise this century from process-based models vary widely[1-6]. In particular, DeConto and Pollard (2016)[6] (here DP16) introduced a hypothesised 'marine ice cliff instability' (MICI) process[7] resulting in mean values exceeding 1 m by 2100 under some methodological choices. However, the DP16 results are sensitive to these choices (Table 1: Mean ± 1 s.d.; Extended Data Figures 1a and b), and the shapes of the probability distributions are very poorly known (Extended Data Figure 2), leading to extremely wide probability intervals (Table 1). This considerable uncertainty poses challenges for robust and cost-effective coastal flood risk management.

The Antarctic contribution to global mean sea-level (GMSL) has two parts: increasing snowfall, which is expected to reduce GMSL by a few centimetres this century, and ice discharge into the ocean, which is very uncertain[1]. The latter is determined by outflow of ice across the 'grounding line' (the boundary between floating and grounded ice), which can increase due to faster ice flow or inland retreat of the grounding line. Ice discharge can increase if buttressing by ice shelves is reduced by (1) ice shelf thinning, caused by enhanced oceanic melting due to circulation changes[8] or direct warming, or (2) partial or total ice shelf collapse, caused by widening of surface crevasses by meltwater due to atmospheric warming[9,10].

Marine parts of the ice sheet, lying on bedrock below sea-level, are potentially vulnerable to two hypothesised positive feedbacks that may have led to past collapse of the West Antarctic ice sheet[11]. Both are based on physical mechanisms with theoretical

foundations, but it is not yet clear the degree to which these could lead to positive feedbacks (i.e. widespread, rapid and sustained ice losses). 'Marine Ice Sheet Instability' (MISI)[12] is a self-sustaining retreat of the grounding line in regions where the bedrock slopes downward inland, triggered by ice shelf thinning or collapse. Ice thickness at the grounding line increases (due to the bedrock slope), leading to faster ice flow, causing further retreat. Satellite and modelling evidence suggests MISI is underway in West Antarctica[13,14,15], though it is unclear the degree to which the driver of this, warm Circumpolar Deep Water breaching the continental shelf, has been affected by human activities[1,16,17]. 'Marine Ice Cliff Instability' (MICI)[6,7] is a self-sustaining retreat of the ice front in regions where the ice is 100 m or more above the ocean surface[18], triggered by ice shelf collapse. These tall ice cliffs are structurally unstable, and their collapse could leave behind further tall cliffs, resulting in sustained ice losses. Observational evidence for MICI is indirect: an absence of ice cliffs taller than 100 m, and rapid retreat of the front of the Jakobshavn (Greenland) and Crane (Antarctic) glaciers (see Knowledge Gaps and Future Directions).

DP16[6] use an Antarctic ice sheet model with a new parameterisation of MICI[7], generating a 64-member ensemble by varying three parameters controlling the relationship between ocean temperature and basal melting, ice shelf disintegration, and maximum rate of ice cliff collapse. They make projections to 2500 under three Representative Concentration Pathways (RCPs): RCP2.6, RCP4.5 and RCP8.5, for very low, low-to-medium and very high greenhouse gas concentrations respectively[1]. They calibrate these by accepting only ensemble members that reproduce reconstructed Antarctic sea-level contributions in the mid-Pliocene (~3 million years ago) and Last Interglacial (LIG: ~130,000–115,000 years ago) eras, and present results for two methodological choices. The first is the Pliocene calibration, using an interval of 5-15 m or 10-20 m; the latter increases sea-level contributions by up to 40 cm by 2100 and 2.5 m by 2500 under RCP8.5 (here "LowPliocene"/"HighPliocene"). The second is an ocean temperature correction of +3°C in West Antarctica to improve simulations of the present ice sheet ("BiasCorrected"/"BiasUncorrected"); this increases sea-level contributions by up to 15 cm this century, but makes little difference by 2500. Results for RCP8.5 at 2100 are given in Table 1; the corresponding distributions are shown in Extended Data Figure 2.

We use statistical techniques for quantifying uncertainties for computationally expensive computer models to re-examine, and estimate probability distributions for, the DP16 projections. We calibrate with the Pliocene, LIG and satellite (1992-2017) eras and make probabilistic projections with and without MICI, comparing with other probabilistic model projections and a Gaussian interpretation of DP16. Finally, we outline knowledge gaps and suggest future directions.

New projections for Antarctica

We estimate probabilistic projections for the Antarctic contribution to sea-level rise by 'emulating' the DP16 ice sheet model (see Methods). This quantifies how a computer model's outputs vary as a function of its input parameters, to predict outputs for any parameter values, enabling us to generate a far larger ensemble than with the original model and to present results both with and without MICI. For this we assume all parameter values are equally likely within the original ranges, based on discussions with the DP16 authors (R. DeConto, pers. comm.). Estimating probability distributions allows meaningful comparison with other studies, and decision-making using sea-level exceedance probabilities under both MICI and No-MICI scenarios. Our method has two further additions: calibration with both palaeodata and satellite data, re-expressing this in the statistical framework of 'history matching' (see Methods), and accounting for ice sheet model error.

Reconstructions of past climate change provide important tests of models, particularly when the changes were large and/or warmer than today, but their uncertainties are typically large and often poorly-defined[19]; recent observations have smaller signals but far smaller uncertainties. The two provide complementary information, so we use both. We use the LowPliocene (equivalent to a combined range of 5-20 m, because the highest simulation is 12.4 m), for two reasons: the large reconstruction uncertainty (values lower than 10 m cannot be ruled out: e.g. a more recent estimate has a maximum of 13 m[20]), and because the DP16 projections are very sensitive to the lower bound of the HighPliocene (Extended Data Figure 2a and b). The 'calibration relationships' between RCP8.5 sea-level contribution at 2100 and sea-level change for the three past eras are shown in Extended Data Figure 3.

To estimate probability distributions we use 'history matching' (HM), where implausible model versions are excluded, rather than the more commonly known Bayesian calibration (BC), where model versions are weighted by their agreement with observations using a likelihood function (metric of model success). This is for several reasons. The concept of HM is the same as DP16, which allows us to make a simpler and more transparent comparison. This method effectively estimates what DP16 would have found if they had substantially greater computing resources, calibrated their ensemble with satellite data, and accounted for model error. History matching is also more 'cautious' than Bayesian model calibration: if no model versions match the data, they are all excluded, while BC retains all and upweights the 'least bad'. Finally, we do not know the shape of the crucial Bayesian likelihood function for the Pliocene and LIG: this would require estimates of the palaeodata

mean and error distribution, rather than assuming all values within the interval are equally likely. Guessing these might shift (wrong mean) or narrow (wrong distribution) the final probability distributions.

Accounting for model error, 'discrepancy'[21], widens the calibration intervals of acceptance (Extended Data Figures 3 and 4: from grey shaded boxes to dashed lines) and is necessary to avoid over-confidence[22,23]: the aim is to account for model structural error and other model uncertainties not sampled in the ensemble. These discrepancy terms are tolerances that reflect how well we expect the ice sheet model to reproduce reality. We specify them using expert judgement, including the judgement that they are greater than reconstruction/observation errors[4,24] (i.e. we judge that confidence in simulating reality with the ice sheet model is lower than in observing or reconstructing it from measurements). Reconstruction errors are not defined by DP16, so we conservatively use half the palaeodata range to avoid underestimating uncertainty (Pliocene: 5 m; LIG: 2 m). For the satellite period, the sea-level change is (0.756 ± 0.386) cm for 1992-2017[25]; we conservatively specify the model error as 0.5 cm.

We present projections at 2100 in Figure 1 and Table 2. The distributions are skewed: modes are consistently lower than medians and means. The results are not strongly dependent on the Pliocene calibration lower bound, unlike the DP16 ensemble, due to the much larger ensemble size (Extended Data Figure 2c: RCP8.5 at 2100 with MICI). Emulated projections without MICI are much lower than those with MICI, and are consistent with previous projections by Ritz et al. (2015)[4] (Figure 1b). The results are robust to changes in calibration era and discrepancy (Extended Data Figure 5).

Crucially, our results show ice cliff instability is not required to reproduce sea-level changes in these three very different eras: 55% of the MICI and 51% of the No-MICI emulator ensemble members simultaneously pass calibration with the Pliocene, LIG and satellite eras (Extended Data Figure 4: larger emulator blue circles within dashed box). MICI increases the ensemble range to encompass more of the data intervals, but the emulator can identify many more areas of the model's parameter space that are successful: including many without MICI. MICI is therefore not necessary for realistic simulations of these periods, so this positive feedback hypothesis cannot be confirmed or ruled out with this data and calibration method. In fact, the Pliocene does not rule out any ensemble members, because accounting for model error widens the calibration interval to accept them all (Extended Data Figure 3a).

The original DP16 projections have substantial probabilities of net sea-level fall this century, with the RCP8.5 LowPliocene mean ± 1 s.d. envelope including negative values

until the 2070s. The emulated projections reflect this (Figure 2), though with lower probability (5th percentile negative until the 2070s). Calibration selects mostly positive sea-level contributions during 1992-2017 (Extended Data Figure 3c), then surface accumulation increases with warming (particularly for RCP8.5) and dominates over ice discharge in many ensemble members during this period.

We estimate when the hypothesised MICI feedback would accelerate sea-level rise. Contributions with MICI quickly start to diverge from those without for all RCPs: in the 2020s (95th percentiles: Figure 2), resulting from the Antarctic Peninsula (DP16: Figure 4c). Dependence of the Antarctic contribution on RCP with MICI begins mid-century, while emergence of a clear, RCP-dependent signal without MICI begins in the 2060s-2070s.

We apply the same emulation and calibration methods to the full DP16 time series (Figure 3a). The RCP8.5 distribution remains very skewed, with the mode at the low end of the range; the same is true of RCP4.5, until the 2340s when the mode jumps to the high end of the distribution (from 1.7 m to 4.6 m) and remains there (as seen for 2500). Virtually all the long-term uncertainty arises from MICI. The No-MICI projections remain narrow over multiple centuries – particularly for RCP8.5, which becomes more narrow – because the sea-level contribution in the DP16 ensemble depends less on the parameters controlling ice shelf vulnerability and basal melting over the long-term than during this century. This suggests the DP16 ensemble either seriously under-samples model uncertainties relevant to long-term change, or the model is structurally deficient because the sensitivity to important parameters diminishes under warming. We therefore consider the post-2100 projections to be less reliable.

The projected probabilities of exceeding 1 m sea-level contribution over time are shown in Figure 3b. These show that, for high probabilities of first exceeding 1 m Antarctic contribution to sea-level, the difference in exceedance time between RCP8.5 and RCP4.5 greenhouse gas concentration scenarios is generally much greater than between projections with or without MICI under RCP8.5. They also show that RCP2.6, i.e. strong mitigation of greenhouse gas concentrations broadly consistent with the 2015 Paris Agreement, is the only one of these scenarios to ensure a low probability of high sea-level rise.

Multi-model comparisons

Figure 4 compares the emulated projections at 2100 under RCP8.5 and RCP2.6 with other studies. We compare only with probabilistic projections[2-5], because these have a clear interpretation, and studies that incorporate at least some process-based modelling (rather than

only expert elicitation or extrapolation), because we are interested in physical modelling uncertainties and we expect the Antarctica to be governed by different processes in the future than the past (which is not accounted for in extrapolation).

We find the emulated No-MICI results agree well with other studies: 95th percentiles are around 30-40 cm under high scenarios and 10-20 cm under low scenarios, despite the use of very different models and approaches (and some differences in scenario and contribution definitions; see Methods). A recent projection by Golledge et al. (2018)[26] incorporating ice-ocean-atmosphere feedbacks is also consistent (14 cm under RCP8.5. compared with DP16-based mode of 15 cm; emergence of signal from mid-century). The No-MICI projections for RCP4.5 are very similar to the IPCC (2013) assessment for 2100 relative to 1986–2005[1] (Emulated DP16: 5 [–1, 15] cm median and 66% probability interval; IPCC: 5 [–5, 15] cm median and 66% or greater probability). The IPCC (2013) estimates for Antarctic ice discharge do not depend on greenhouse gas scenario, so the projections for RCP2.6 are slightly lower than the IPCC (Emulated DP16: –1 [–7, 7] cm, IPCC: 6 [–4, 16] cm) and higher for RCP8.5 (Emulated DP16: 21 [13, 31] cm, IPCC: 4 [–8, 14] cm).

Le Bars et al. (2017)[27] make probabilistic interpretations of DP16 for assessing high-end total GMSL by taking the HighPliocene BiasCorrected mean and standard deviation and assuming the distribution is Gaussian. This gives probabilities of exceeding 0.5 m and 1 m Antarctic contribution by 2100 under RCP8.5 of 96% and 65%, respectively. We argue this interpretation is not justifiable, as the original DP16 distributions are skewed (Extended Data Figure 2) and the HighPliocene constraint is not robust (discussed above). Using minimal assumptions about the distribution shape instead would mean probability intervals were very poorly constrained (Table 1). Our estimates of the distribution shape give lower exceedance probabilities: 71% and 36%, respectively (Table 2); We conclude that, although significant sea-level rise is possible under the probability distributions estimated from DP16, Le Bars et al. (2017) systematically overestimate the probability of high sea-level contribution from Antarctica this century.

Only Ritz et al. (2015)[4] have made probabilistic projections beyond 2100. At 2200, the emulated No-MICI projections under RCP8.5 are an order of magnitude higher than Ritz et al. (2015) projections under the medium-high A1B scenario (Figure 3a; emulated median and 90% probability interval: 4.0 [3.7, 4.2] m; Ritz et al. (2015): 0.41 [0.04, 0.72] m) and more than double the projections by Golledge et al. (2015)[28] for RCP8.5 (0.88 m and 1.52 m at 2200 for two model versions). Beyond 2200, the DP16-derived projections under RCP8.5 become increasingly inconsistent with Golledge et al. (2015) (Figure 3a). The 2.5th percentile at 2500 without MICI is higher than the latter's projections at 2500 even under a doubling of

RCP8.5 temperature changes. This is particularly surprising, given DP16 greenhouse gas concentrations are capped from the year 2175. However, the RCP4.5 and RCP2.6 No-MICI projections are consistent: the Golledge et al. (2015) ranges fall within the 90% probability intervals.

This suggests the DP16 model may be over-sensitive to very large atmospheric temperature changes, even without MICI: i.e. the response is not self-limiting, due to widespread ice shelf sensitivity to warming and/or a lack of local factors mitigating MISI (e.g. bedrock topography, basal traction and sliding, theoretical constraints on ice stresses at the grounding line, and predicted climatic triggers), in contrast to findings from a diversity of other ice sheet and ice shelf models[4,9,14,15,28,29].

Knowledge gaps and future directions

Our analysis has two aims: to make best estimates of the probability distributions implied by the DP16 study and satellite record, and to evaluate ways in which the original study could be built upon to improve confidence in Antarctic projections. Altering the DP16 climate or ice sheet models, and extending the ensemble parameter ranges, are beyond the scope of this study. For example, we could test the effect of reducing the range of the ice cliff collapse parameter VCLIF (Extended Data Figure 5), but not increasing it. These estimates therefore incorporate many of the limitations of DP16, and should be seen as a first step towards a full assessment of Antarctic sea-level uncertainty.

We made pragmatic, simple choices, such as using the same palaeodata intervals as DP16 and uniform distributions for the parameters. Future work should explore alternatives: sampling of the parameter space, palaeodata reconstructions with well-defined uncertainty estimates, spatio-temporal patterns from satellite data, and Bayesian calibration. We are confident that the tails of the sea-level distributions (essential to decision-making) have not been truncated too much by the calibration, as we use a 99.7% probability interval for the satellite data (see Methods) and the palaeodata have very little influence (Extended Data Figure 5). Nevertheless we present projections only to the 95th percentile, to reflect our judgement about the precision of these estimates. Most importantly, presence or absence of MICI is by far the largest uncertainty in sea-level rise this century that could be quantified in this study.

Although the maximum height of ice cliffs is founded in theory and indirectly supported by observations and geological evidence[18,30], very little is known about whether initial cliff collapse would lead to a positive feedback (i.e. MICI), how this would vary in

different locations, the consequent rate of ice wastage, and how long it would last. MICI might be mitigated by cool, fresh meltwater entering the ocean, buttressing by ice mélange, or changes in relative sea-level from gravitational and solid earth effects. Greenland's Helheim and Jakobshavn glaciers have high rates of ice wastage, but this is dominated by their fast flow, not grounding line retreat. Reducing the maximum ice wastage value by 20% to 4 km/a reduces the RCP8.5 projected median by 14% and the 95th percentile by 17% (Extended Data Figure 5), and higher maximum values (which it is not possible to explore in this study) would likely have the opposite effect. The parameterisation of ice loss by MICI in DP16 is very simple, and the low resolution of the model might also over-estimate the occurrence of tall cliffs. A diversity of model parameterisations is therefore needed.

Triggers are also poorly understood. DP16 predict early and widespread surface melting (DP16: Extended Data Figure 4) and ice shelf collapse, due to high atmospheric warming, high sensitivity of melting/collapse to warming, or both. This is in contrast with studies using process-based models, which predict up to 5-6 times less surface melting around the Peninsula and 3-8 times less on the West Antarctic Abbot ice shelf by 2100 under RCP8.5[10], and that only shelves along the Peninsula are vulnerable this century under SRES A1B[9] and RCP8.5[10]. Observational evidence of ice shelf melting has highlighted both amplifying and mitigating processes[31-33], and atmosphere and ocean models have limitations such as present day biases and missing processes, so further process studies and monitoring are required. The DP16 model shows low sensitivity to ocean melting (DP16 Figure 6) and apparently unconstrained response to atmospheric warming (Figure 3a), in contrast with other models[4,9,14,15,28,29,34]. Again, a greater diversity of models is needed, along with standardised extension of greenhouse gas concentration scenarios, in order to estimate ice sheet stability on multi-centennial timescales. For the Pliocene, DP16 apply a 2°C ocean warming but Golledge et al. (2017)[35] estimate this was 3°C, so the contribution to sea-level rise may be under-estimated.

Using palaeo-reconstructions to calibrate models requires robust quantification of their uncertainties. History matching calibrations typically use a mean ± 3 s.d. interval, which for continuous and unimodal distributions corresponds to 95% or greater probability[36] for calibration with one observation. For the Pliocene, total GMSL change reconstructed by Miller et al. (2012)[37] implies an Antarctic contribution of approximately 4-24 m (95% range), Gasson et al. (2016)[20] estimated an Antarctic contribution of -1 to 13 m (with less confidence in the lower bound), Golledge et al. (2017)[35] estimated an Antarctic contribution in the early Pliocene of 3-14.2 m (95% range) – all equivalent to, or wider than, the interval used here (i.e. no constraint) – while Raymo et al. (2018)[38] argue that Pliocene GMSL is effectively

unknown. For the LIG, we have assumed the DP16 range (3.5-7.4 m) is sufficiently broad, but the GMSL estimate by Kopp et al. (2013)[39] implies a 90% interval for Antarctica of around 1.6-7.5 m, while the 80% probability interval implied by Dusterhus et al. (2016)[40] (1.3-13.3 m) would virtually eliminate the LIG as a constraint. Long-term deformations in the earth's surface have also recently been estimated to potentially increase estimates of total GMSL at the LIG by up to several metres[41]. In fact, emulated projections calibrated only with the satellite period are virtually identical to those calibrated with all three eras (Extended Data Figure 5), indicating that these evaluations with palaeodata have little impact. Using Bayesian calibration (weighting ensemble members by their difference with the data) might yield a stronger constraint, but this would require estimates of mean values and error distributions (e.g. Gaussian).

The DP16 ensemble design is not optimal: it includes large gaps and effectively duplicated simulations, and under-samples model uncertainties. Failing to incorporate model error in the calibration also means their projections are likely too narrow and over-confident, a problem amplified by sensitivity to the Pliocene lower bound. Ensemble designs should be space-filling[4,42] and test which uncertainties are most important to sample (e.g. 'pre-calibration'[43,44]); emulation allows efficient ensemble design and sensitivity analysis. Statistically-meaningful calibrations (such as history matching and Bayesian updating, with model discrepancy) improves interpretation of the data constraints and robustness and interpretation of the resulting projections.

Currently there are few probabilistic Antarctic model projections, and they assess different uncertainties in different ways. We propose a new vision of a 'grand ensemble' designed across multiple diverse ice sheet models simultaneously, systematically sampling parameters, structures, boundary conditions and initial conditions[34]. Co-ordinated design would allow multi-model emulation, a statistically rigorous method of interpreting and combining different model projections, to estimate probability distributions that account for multiple model structural uncertainties. The Ice Sheet Model Intercomparison Project (ISMIP6) is bringing together an international consortium of ice sheet modellers to make projections for the Greenland and Antarctic ice sheets[45]; this presents an ideal opportunity to design such a framework.

References

1. IPCC. *Working Group I Contribution to the IPCC Fifth Assessment Report Climate Change 2013: The Physical Science Basis*. (Cambridge University Press, 2013).
2. Little, C. M., Oppenheimer, M. & Urban, N. M. Upper bounds on twenty-first-century Antarctic ice loss assessed using a probabilistic framework. *Nature Climate Change* 3, 1–6 (2013).
3. Levermann, A. *et al.* Projecting Antarctic ice discharge using response functions from SeaRISE ice-sheet models. *Earth Syst. Dynam.* 5, 271–293 (2014).
4. Ritz, C. *et al.* Potential sea-level rise from Antarctic ice-sheet instability constrained by observations. *Nature* 528, 115–118 (2015).
5. Ruckert, K. L. *et al.* Assessing the Impact of Retreat Mechanisms in a Simple Antarctic Ice Sheet Model Using Bayesian Calibration. *PLOS ONE* 12, e0170052 (2016).
6. DeConto, R. M. & Pollard, D. Contribution of Antarctica to past and future sea-level rise. *Nature* 531, 591–597 (2016).
7. Pollard, D., DeConto, R. M. & Alley, R. B. Potential Antarctic Ice Sheet retreat driven by hydrofracturing and ice cliff failure. *Earth and Planetary Science Letters* 412, 112–121 (2015).
8. Hellmer, H. H., Kauker, F., Timmermann, R., Determann, J. & Rae, J. Twenty-first-century warming of a large Antarctic ice-shelf cavity by a redirected coastal current. *Nature* 485, 225–228 (2012).
9. Kuipers Munneke, P., Ligtenberg, S. R. M., Van den Broeke, M. R. & Vaughan, D. G. Firn air depletion as a precursor of Antarctic ice-shelf collapse. *Journal of Glaciology* 60, 205–214 (2014).
10. Trusel, L.D. *et al*. Divergent trajectories of Antarctic surface melt under two twenty-first-century climate scenarios. *Nature Geoscience*, 8(12), pp.927–932 (2015).
11. Vaughan, D. G. West Antarctic Ice Sheet collapse – the fall and rise of a paradigm. *Climatic Change* 91, 65–79 (2008).
12. Schoof, C. Ice sheet grounding line dynamics: Steady states, stability, and hysteresis. *Journal of Geophysical Research* 112, F03S28 (2007).
13. Rignot, E., Mouginot, J., Morlighem, M., Seroussi, H. & Scheuchl, B. Widespread, rapid grounding line retreat of Pine Island, Thwaites, Smith, and Kohler glaciers, West Antarctica, from 1992 to 2011. *Geophysical Research Letters* 41, 3502–3509 (2014).
14. Favier, L. *et al.* Retreat of Pine Island Glacier controlled by marine ice-sheet instability. *Nature Climate Change* 5, 117–121 (2014).
15. Joughin, I., Smith, B. E. & Medley, B. Marine Ice Sheet Collapse Potentially Under Way for the Thwaites Glacier Basin, West Antarctica. *Science* 344, 735–738 (2014).
16. Waugh, D. W., Primeau, F., DeVries, T. & Holzer, M. Recent Changes in the Ventilation of the Southern Oceans. *Science* 339, 568–570 (2013).
17. Previdi, M. & Polvani, L. M. Climate system response to stratospheric ozone depletion and recovery. *Q J Roy Meteor Soc* 140, 2401–2419 (2014).
18. Bassis, J. N. & Walker, C. C. Upper and lower limits on the stability of calving glaciers from the yield strength envelope of ice. *Proceedings of the Royal Society A: Mathematical, Physical and Engineering Sciences* 468, 913–931 (2012).
19. Sweeney, J., Salter-Townshend, M., Edwards, T., Buck, C. E. & Parnell, A. C. Statistical Challenges in Estimating Past Climate Changes. *WIREs Computational Statistics*, 10 (5), e1437 (2018).

https://doi.org/10.1002/wics.1437
20. Gasson, E., DeConto, R. M. & Pollard, D. Modeling the oxygen isotope composition of the Antarctic ice sheet and its significance to Pliocene sea-level. *Geology* 44, 827–830 (2016).
21. Williamson, D., Blaker, A., Hampton, C. & Salter, J. Identifying and removing structural biases in climate models with history matching. *Climate Dynamics* 45, 1299–1324 (2014).
22. McNeall, D. *et al.* The impact of structural error on parameter constraint in a climate model. *Earth Syst. Dynam.* 7, 917–935 (2016).
23. Williamson, D., Blaker, A. T. & Sinha, B. Tuning without over-tuning: parametric uncertainty quantification for the NEMO ocean model. *Geosci. Model Dev.* 10, 1789–1816 (2017). doi:10.5194/gmd-2016-185-AC3
24. Gladstone, R. M. *et al.* Calibrated prediction of Pine Island Glacier retreat during the 21st and 22nd centuries with a coupled flowline model. *Earth and Planetary Science Letters* 333-334, 191–199 (2012).
25. Shepherd, A. *et al.* Mass balance of the Antarctic Ice Sheet from 1992 to 2017. *Nature* 558, 219–222 (2018).
26. Golledge, N., E. D. Keller, N. Gomez, K. A. Naughten, J. Bernales, L. D. Trusel, and T. L. Edwards (2018), Causes and consequences of 21st century ice sheet melt. *Submitted*.
27. Le Bars, D., Drijfhout, S. & de Vries, H. A high-end sea-level rise probabilistic projection including rapid Antarctic ice sheet mass loss. *Environ Res Lett* 12, 044013 (2017).
28. Golledge, N. R. *et al.* The multi-millennial Antarctic commitment to future sea-level rise. *Nature* 526, 421–425 (2015).
29. Cornford, S. L. *et al.* Century-scale simulations of the response of the West Antarctic Ice Sheet to a warming climate. *The Cryosphere* 9, 1579–1600– (2015).
30. Wise, M. G., Dowdeswell, J. A., Jakobsson, M. & Larter, R. D. Evidence of marine ice-cliff instability in PineIsland Bay from iceberg-keel plough marks. *Nature* 550, 506–510 (2017).
31. Bell, R. E. *et al.* Antarctic ice shelf potentially stabilized by export of meltwater in surface river. *Nature* 544, 344–348 (2017).
32. Kingslake, J., Ely, J. C., Das, I. & Bell, R. E. Widespread movement of meltwater onto and across Antarctic ice shelves. *Nature* 544, 349–352 (2017).
33. Gourmelen, N. *et al.* Channelized Melting Drives Thinning Under a Rapidly Melting Antarctic Ice Shelf. *Geophysical Research Letters* 17, 173 (2017).
34. Pattyn, F., Favier, L., Sun, S. & Durand, G. Progress in Numerical Modeling of Antarctic Ice-Sheet Dynamics. *Curr Clim Change Rep* 3, 174–184 (2017).
35. Golledge et al. (2017), Antarctic climate and ice-sheet configuration during the early Pliocene interglacial at 4.23 Ma, *Climate of the Past*, 13(7), pp.959–975.
36. Pukelsheim, F. The three sigma rule. *The American Statistician* 48, 88–91 (1994).
37. Miller, K. G. *et al.* High tide of the warm Pliocene: Implications of global sea-level for Antarctic deglaciation. *Geology* 40, 407–410 (2012).
38. Raymo, M.E. et al., 2018. The accuracy of mid-Pliocene δ18O-based ice volume and sea level reconstructions. *Earth-Science Reviews*, 177, pp.291–302.
39. Kopp, R. E., Simons, F. J., Mitrovica, J. X., Maloof, A. C. & Oppenheimer, M. A probabilistic assessment of sea-level variations within the last interglacial stage. *Geophysical Journal International* 193, 711–716 (2013).
40. Düsterhus, André, Tamisiea, M. E. & Jevrejeva, S. Estimating the sea-level highstand during the Last Interglacial: a probabilistic massive ensemble

approach. *Geophysical Journal International* 206, 900–920 (2016).
41. Austermann, J., Mitrovica, J. X., Huybers, P. & Rovere, A. Detection of a dynamic topography signal in last interglacial sea-level records. *Science Advances* 3, 1–9 (2017).
42. Nias, I., Cornford, S. L. & Payne, A. J. Contrasting model sensitivity of the Amundsen Sea embayment ice streams. *Journal of Glaciology* 62, 552–562 (2016).
43. Holden, P. B., Edwards, N. R., Oliver, K. I. C., Lenton, T. M. & Wilkinson, R. D. A probabilistic calibration of climate sensitivity and terrestrial carbon change in GENIE-1. *Climate Dynamics* 35, 785–806 (2009).
44. Edwards, N. R., Cameron, D. & Rougier, J. Precalibrating an intermediate complexity climate model. *Climate Dynamics* 37, 1469–1482 (2011).
45. Nowicki, S. M. J. *et al.* Ice Sheet Model Intercomparison Project (ISMIP6) contribution to CMIP6. *Geosci. Model Dev. Discuss.* 1–42 (2016). doi:10.5194/gmd-2016-105-SC2

Acknowledgements

T.L.E., N.E. and P.H. were supported by EPSRC REsearch on Changes of Variability and Environmental Risk (ReCoVER: EP/M008495/1) under the Quantifying Uncertainty in ANTarctic Ice Sheet instability (QUAntIS) project (RFFLP 006). T.L.E. was also supported by the EPSRC-funded Past Earth Network (EP/M008363/1) and the Université Joseph Fourier – Grenoble International visitor fund 'Campagne INVITES'. N.R.G is supported by contract VUW1501 from the Royal Society Te Aparangi. I.N. was supported by the NERC iSTAR-C project Dynamical control on the response of Pine Island Glacier (NE/J005738/1) and now by the NASA Sea Level Change program. A.W. is supported by the Open University Faculty of Science, Technology, Engineering and Mathematics.

Thanks to Rob DeConto for running additional simulations necessary for the analysis, suggestions and helpful discussions, and to Kelsey Ruckert and Anders Levermann for providing data. Thanks to the statisticans who attended the Past Earth Network events 'Assessing Palaeoclimate Uncertainty' (held jointly with the Environmental Statistics Section of the Royal Statistics Society, Cambridge, August 2016), 'Emulators workshop' (Leeds, June 2017), and writing retreat (Callow Hall, August 2017) for their advice, particularly Ian Vernon, Peter Challenor, and Jonty Rougier. Thanks to Dewi Le Bars, Doug McNeall, David Demeritt and the King's Geography Hazards, Risk and Regulation reading group (George Adamson, Felicia Liu, Amar Razli, Laurence Ball and Ana Heilbron) for helpful comments on the manuscript. Thanks to three anonymous reviewers for their comments and advice. Thanks also to Dr Kai-Keen Shiu of the Gastrointestinal Oncology Unit at UCL Hospitals, and to Dallas Campbell without whom this work would not have been possible.

Author contributions

T.L.E. conceived the idea, carried out the analysis, produced the figures, and wrote the manuscript. A.W. and P.B.H. performed preliminary analyses. A.J.P, A.W., C.R., G.D., I.N., M.B. and N.R.G. contributed ideas on glaciological and oceanic aspects, while A.W., N.R.E. and P.B.H. contributed ideas on statistical aspects. All authors contributed to writing the manuscript.

Author information

The authors declare no competing financial interests. Correspondence and requests for materials should be addressed to T.L.E. (tamsin.edwards@kcl.ac.uk).

Table 1. Probabilities from DeConto and Pollard (2016) study. Means and standard deviations, and implied probability intervals, for DeConto and Pollard (2016) ensemble at 2100 for RCP8.5 for their four methodological choices (see text), using minimal assumptions about the distribution shape (finite mean and variance: Chebyshev inequality).

RCP8.5	**LOW PLIOCENE**		**HIGH PLIOCENE**	
	Bias Uncorrected	**Bias Corrected**	**Bias Uncorrected**	**Bias Corrected**
Antarctic contribution at 2100 (cm sea-level equivalent)				
Mean ± 1 s.d.	64 ± 49	79 ± 46	105 ± 30	114 ± 36
≥ 68% probability interval	[-22, 150]	[-2, 160]	[51, 158]	[51, 177]
≥ 90% probability interval	[-90, 217]	[-65, 223]	[9, 200]	[1, 227]

Table 2. Projections for the Antarctic contribution to sea-level in 2100. Calibrated with Pliocene, Last Interglacial and satellite data (1997-2017), with and without DeConto and Pollard (2016) marine ice cliff instability (MICI) parameterisation.

	RCP2.6		RCP4.5		RCP8.5	
	No MICI	**MICI**	**No MICI**	**MICI**	**No MICI**	**MICI**
Antarctic contribution at 2100 (cm sea-level equivalent)						
Mode	-6	15	0	24	15	45
Median	-1	19	5	46	21	79
Mean	0	20	7	49	22	83
68% interval	[-7, 8]	[4, 36]	[-1, 15]	[16, 83]	[13, 32]	[35, 133]
90% interval	[-9, 13]	[-3, 48]	[-3, 21]	[5, 103]	[9, 39]	[20, 157]
Exceedance probabilities						
≥ 30 cm	--	26%	--	68%	20%	88%
≥ 50 cm	--	4%	--	46%	--	71%
≥ 1 m	--	--	--	6%	--	36%

Figure 1. Probabilistic projections of the Antarctic contribution to sea-level at 2100. Projections estimated under three RCPs, (a) with ice cliff instability parameterisation and (b) without, from emulation of the DeConto and Pollard (2016) ice sheet model ensemble. Dotted lines are the uncalibrated emulator ensemble; solid lines are calibrated with Last Interglacial and Pliocene reconstructions and satellite data from 1992-2017. Box and whiskers show the [5, 25, 50, 75, 95]th percentiles; star shows the mode. The DeConto and Pollard (2016) ensemble members for RCP8.5 (LowPliocene calibration; BiasCorrected and BiasUncorrected combined) are shown as a histogram and mean ± 2 s.d. interval in (a), scaled to the same height as the calibrated projection. The projection for the Antarctic contribution due to ice discharge under the medium-high climate scenario A1B by Ritz et al. (2015) is also shown in (b). Data from refs. 6 and 25 and supplementary simulations by R. DeConto (pers. comm.) (see Methods).

Figure 2. **Emergence of ice cliff instability.** Projected 5-95% probability intervals for Antarctic sea-level contributions this century, with and without the marine ice cliff instability (MICI) parameterisation of DeConto and Pollard (2016). Data from refs. 6 and 25 and supplementary simulations by R. DeConto (pers. comm.) (see Methods).

Figure 3. Long-term projections of Antarctic sea-level contribution. (a) Shaded/hatched regions: projected 5-95% intervals for Antarctic sea-level contribution to 2300 and for 2500 with (shaded) and without (hatched) ice cliff instability (MICI) parameterisation under three greenhouse gas concentration scenarios. Dots: mode of the RCP4.5 and RCP8.5 distributions with MICI. Single lines: range of results from Golledge et al. (2015) under RCP8.5 (solid dark red), RCP8.5 with doubled atmosphere and ocean temperature changes (dashed purple), RCP4.5 and RCP2.6 (solid black). Box and whisker at 2200 shows Ritz et al. (2015): [5, 25, 50, 75, 95]th percentiles and mode (*). (b). Projected probability of exceeding 1 m Antarctic sea-level contribution over the same period. Data from refs. 6 and 25 and supplementary simulations by R. DeConto (pers. comm.) (see Methods).

Figure 4. Multi-model comparison. Projections from this study (bold text: 'EMULATED') at 2100 based on emulation of DeConto and Pollard (2016) (with and without ice cliff instability, 'MICI'), along with results from other probabilistic modelling studies. Box and whiskers show the [5, 25, 50, 75, 95]th percentiles; star shows the mode. Numbers show the median, [5th, 95th] percentiles and, where available, the mode (*). "High Scenarios" (pink/red) are for high-end (RCP8.5) or medium-high (Special Report on Emissions Scenario A1B[1]) greenhouse gas emissions or concentrations, or immediate collapse of part of West Antarctica (Little et al. (2013): 5th percentile and median are estimated from digitisation); Levermann et al. (2014) is from models with ice shelves, without time delay. "Low Scenarios" (grey/black) are for low greenhouse gas concentrations (RCP2.6) or other baseline case (Little et al., 2013); Levermann et al. (2014) is with time delay. Levermann et al. (2014) and Ritz et al. (2015) are for ice discharge contribution only. Data from refs. 2-6 and 25, supplementary simulations by R. DeConto (pers. comm.), and mode for ref. 5 supplied by K.L. Ruckert (pers. comm) (see Methods).

METHODS

Simulator ensemble design

DeConto and Pollard (2016) perturb three continuous parameters, sampling four levels for each in a factorial design to generate $4^3 = 64$ ensemble members:

OCFAC: Ocean melt factor, which controls sub-ice-shelf direct melting. Defined as a factor by which the default value is multiplied. OCFAC = {0.1, 1, 3 and 10} x 0.224 m yr^{-1} $°C^{-2}$. (Note that DP16 quotes incorrect units of m yr^{-2} $°C^{-2}$ in two places).

CREVLIQ: Crevasse liquid depth, which controls ice shelf collapse by hydrofracturing due to surface liquid. Defined as the additional crevasse depth due to surface melt plus rainfall rate. CREVLIQ = {0, 50, 100, 150} m per $(m\ yr^{-1})^{-2}$.

VCLIF: Maximum net ice wastage rate. Controls cliff failure after ice shelf collapse. VCLIF = {0, 1, 3, 5}km yr^{-1}.

For present day and future projections, this ensemble is duplicated with the ocean bias correction applied. When emulating the ice sheet model (see below) we combine these 128 ensemble members and treat the bias correction as a continuous uncertain parameter:

BIAS: Southern Ocean bias correction applied to present day and future simulations. Defined as a scalar ranging from 0 (no bias correction, +0°C) to 1 (full bias correction, +3°C). Active only for present day and future simulations.

We use time series data for the ensemble provided by Rob DeConto. When emulating the model, we found a sign error in the DP16 Supplementary Information: the Last Interglacial value for simulation row 6 (OCFAC = 0.1, CREVLIQ = 50, VCLIF = 1) should be +2.63 m, not -2.63 m.

Building the emulators

We use Gaussian Process regression ('kriging' when used for spatial interpolation), because it is flexible, non-parametric, and provides uncertainty estimates[46]. As usual for emulation of computer models, we set the 'nugget' to zero because the ice sheet model is deterministic. We refer to 'the emulator' in the main text for simplicity, but this comprises separate emulators for each scalar output: Pliocene and LIG sea-level change, present day (1992-2017 change in the RCP4.5 simulation) and the change from 2000 to every even-numbered year up to 2500 for the three RCPs. We construct, validate, calibrate and make predictions using the R software packages DiceKriging and a modified version of DiceEvaluation.

Let the function $f(x)$ be the ice sheet model, which simulates sea-level change in a particular era (e.g. the Pliocene) as a function of the set of its input parameters, x. We

consider only one output at a time, to avoid the need for a further index. An emulator $f_{em}(x)$ for a particular output of $f(x)$ can be written as:

$$f_{em}(x) = \sum_j \beta_j g_j(x) + u(x)$$

where $g(x)$ are known functions of x, β are regression coefficients, and $u(x)$ is a stochastic process with a specified covariance function. We wish to select the subset of x that has the most influence on $f_{em}(x)$.

Design and validation of the emulators comprises two parts: a step-wise model selection procedure, to choose the mean function (i.e. which simulator parameters, and interactions between these, to use as regressors), and a 'leave-one-out' (LOO) cross-validation procedure, to evaluate which is the most suitable covariance function and whether each emulator is sufficiently accurate for our purposes. We perform these procedures for six outputs — the two palaeo-eras, the present day, and the three RCP projections at 2100 — to choose the overall emulator structure. The final fitting of the emulators with the full ensemble data, and their use for prediction, are discussed later.

Mean functions: There are important interactions between parameters — for example, increasing the bias correction (BIAS) increases the effect of maximum ice wastage rate (VCLIF) on projections — but we also wish to avoid over-fitting by including too many interaction terms. We use the R MASS package's stepAIC to select model terms, testing up to second order (three-way) interactions between parameters, using Bayesian Information Criterion because it is generally more parsimonious than Akaike Information Criterion. The resulting mean functions for the six outputs are:

Pliocene and Last Interglacial:

$g_{palaeo}(x) \sim$ (OCFAC, CREVLIQ, VCLIF, CREVLIQ*VCLIF)

Present day and RCP2.6 at 2100:

$g_{low}(x) \sim$ (OCFAC, CREVLIQ, VCLIF, BIAS, OCFAC*VCLIF, OCFAC*BIAS, CREVLIQ*VCLIF, VCLIF*BIAS, OCFAC*VCLIF*BIAS)

RCP4.5 and RCP8.5 at 2100:

$g_{high}(x) \sim$ (OCFAC, CREVLIQ, VCLIF, BIAS, OCFAC*VCLIF, OCFAC*BIAS, CREVLIQ*VCLIF)

where *g ~ (a,b)* means *g* is a linear function of *a* and *b,* etc, and *a*b* indicates an interaction term.

Covariance functions: The covariance controls the smoothness between data points, with a trade-off between accuracy and over-fitting. We compare the success of different covariance functions — Matern(5/2), Matern(3/2), exponential, and power-exponential (exponential family, where the exponent can vary between 0 and 2) — using the mean function selected above, and choose the one with the smallest normalised Euclidean distance in a LOO procedure. The LOO procedure comprises fitting the emulator to all ensemble members except one (i.e. 63 of 64 for Pliocene and LIG; 127 of 128 for present and future), and then predicting the final member to compare with the simulation itself. This is repeated for all combinations (N_{ens} = 64 or 128) to provide a summary statistic. Normalised Euclidean distance is:

$$\mathrm{d} = \sqrt{\sum_{\mathrm{i}=1}^{\mathrm{N_{ens}}} \frac{(\mathrm{f_{em}(x_i)} - \mathrm{f(x_i)})^2}{\sigma^2_{\mathrm{em:x_i}}}}$$

,

where *i* is the ensemble member and σ_{em} is the emulator error for that prediction. We choose this metric because it makes use of the uncertainty estimate inherent in a Gaussian Process emulator to standardise the residuals, so that an emulator with some large errors is not overly penalised if it has sufficiently large uncertainty estimates to generally encompass the true value. This also guards against overfitting, by penalising too-confident emulators. The distance metric therefore balances the two aims of emulator accuracy and appropriate confidence. The resulting covariance functions from this procedure are power-exponential for the LIG, Matern(3/2) for 1992-2017, and exponential for the Pliocene and future outputs.

Validating and fitting the emulators

We use various validation outputs to assess emulator adequacy: RMSE; Kendall's tau, a non-parametric measure of correlation, for the emulator predictions versus the simulations; and the fraction of predictions for which the simulation lies within the emulator 95% credibility interval, for which values lower than ~90% would indicate an over-confident emulator (i.e. too-small uncertainty estimates). The RMSE and Kendall rank correlation coefficients between the emulator predictions and simulations are 12 cm (1.4% of the data range) and 0.958 respectively for the Pliocene; 26 cm (2.7%) and 0.923 for the Last Interglacial; 0.1 cm (0.6%) and 0.972 for the present day, and 0.9-1.2 cm (0.4-0.8%) and 0.973-0.976 for the

three future projection emulators, indicating sufficient accuracy. The fraction of predictions within the emulator 95% interval is 100% for the Pliocene, 89% for the LIG, and 91-98% for the present and future, indicating sufficiently large emulator uncertainty estimates. The predictive accuracy and uncertainty estimates of the six emulators can also be inspected visually by plotting the emulator predictions vs simulations and the standardised residuals (Extended Data Figure 6).

Having judged these six emulators to be adequate, we fit each emulator with the full ensemble for that output. We use the emulator structures for the year 2100 for all timeslices for that RCP.

Emulator ensemble design

We predict 10,000 points in the parameter space using a maximin Latin Hypercube (i.e. efficiently space-filling) design. The MICI design samples from uniform distributions for all four parameters, based on discussion with one of the original DP16 authors (DeConto, pers. comm.); the No-MICI design has VCLIF set to zero. The effect of VCLIF, CREVLIQ and OCFAC on sea-level contribution at 2100 under RCP8.5 in the MICI case is shown in Extended Data Figure 7, which shows the strong dependence on VCLIF. The reason for some apparent gaps in emulator coverage is that the ensemble design is space-filling but does not necessarily sample points in each corner of the parameter space, as the original ensemble members do.

Pliocene calibration

The LowPliocene and HighPliocene projections of DP16 are presented (and have been interpreted by others[27,47]) as equally plausible, but here we make the case that the HighPliocene calibration is not robust. This is important because the RCP8.5 projections are uniquely sensitive to the particular minimum value chosen for the HighPliocene constraint (10 m). Extended Data Figure 2a and b show that when the lower bound exceeds 9.6 m, this results in much higher means and much smaller standard deviations, because fewer than a quarter of the ensemble members pass. The sensitivity is caused by a combination of the small ensemble size and the strong correlation in the model between Pliocene sea-level and RCP8.5 projections (large circles in Extended Data Figure 3a).

This sensitivity to the Pliocene lower bound is exacerbated by the choice of calibration method: a simple ‘accept’ or ‘reject’, which can be expressed in the ‘history matching’ framework[22,48] below. This binary filtering means we should choose a sufficiently wide range of tolerance, because every rejected ensemble member is treated as completely implausible

(by being removed, rather than down-weighted as in Bayesian calibration). Treating two ranges as equally plausible is not coherent, because it implies values in the range 5–10 m and 15-20 m are simultaneously both plausible and implausible. The chosen data range should be both broad and unique to obtain a calibration that is robust and meaningful.

Gasson, DeConto and Pollard (2016)[20] estimate the Antarctic contribution to mid-Pliocene sea-level has a maximum of 13 m, which would rule out most of the HighPliocene range, suggesting the interval 10-20 m is not well supported. (A range of 10-13 m would be inconsistent with the large degree of uncertainty in Pliocene reconstructions[37,49])

In fact, increasing the upper bound from 13 m would have no effect, because the maximum Pliocene change in the ensemble is 12.4 m. Decreasing the lower bound below 5 m would also make little difference, because the original (no discrepancy) DP16 Last Interglacial calibration (3.5-7.4 m) rejects these ensemble members: none of the ensemble members that pass the LIG constraint have Pliocene sea-level changes of less than 5 m (Extended Data Figure 4: no large circles directly below shaded box). The crucial judgement is therefore whether the 10 m HighPliocene lower bound can be justified.

We conclude that Pliocene Antarctic sea-level contribution is currently too uncertain to use the HighPliocene constraint, particularly for this model and for a history matching approach, and that the LowPliocene calibration is far more robust.

Model discrepancy

Model 'discrepancy', or 'structural error', is defined as the smallest possible difference between a model simulation and the true values: that is, how well the model could reproduce reality at its best possible, 'tuned', parameter values[4,21,22,23] . Discrepancy is an essential part of model calibration: not incorporating it implies that a model could be tuned to perfectly match reality. Using a value less than the observational error would imply we could simulate reality better than we could measure it. Model discrepancy can, in some cases, be approximately estimated by comparing simulations with multiple observations. But if there are insufficient observations to do this, as is the case here, discrepancy can be viewed as a tolerance to model error[48] estimated by expert judgement[4,24] (see below).

Calibrating projections

We re-express the DP16 calibration within a history matching framework, extending it to account for emulator error and model discrepancy. We adapt notation by Vernon et al. (2010)[50] here. The relationship between a palaeodata reconstruction or an observation of sea-level change (Pliocene, LIG, or 1992-2017 trend), z, and the true value, y, is modelled as:

$$z = y + \epsilon_{obs}$$

where ε_{obs} has variance σ_{obs}^2, the square of the observational or palaeodata reconstruction error. The relationship between the true value and the simulation of this sea-level change is:

$$y = f(x^*) + \epsilon_{md}$$

where x^* are the best values of the parameters, and ε_{md} is the model discrepancy with variance σ_{md}^2. We emulate $f(x)$:

$$f(x) = f_{em}(x) + \epsilon_{em:x}$$

where $f_{em}(x)$ is the mean emulator prediction for $f(x)$, and $\varepsilon_{em:x}$ is the emulator error as before; it varies with x, and is automatically estimated in Gaussian Process emulation. For a given emulated output (Pliocene, LIG, 1992-2017 trend) we can use the standardised distance, also known as *implausibility*, I:

$$\mathcal{I}^2(x) = \frac{(f_{em}(x) - z)^2}{\sigma_{obs}^2 + \sigma_{em:x}^2 + \sigma_{md}^2}$$

to accept or reject a given emulated ensemble member with parameter values x. We interpret the accepted ensemble members as a posterior probability distribution. This represents a judgement that this distribution represents our uncertainty about future sea-level rise (given the limitations of the ice sheet model and palaeodata), i.e. that the parameter space outside the calibration intervals has a low probability of being plausible.

We use a minimum LIG palaeodata value of 3.5 m, rather than the 3.6 m quoted by DP16, for consistency with their calibrated ensemble results which include a member with LIG sea-level change of 3.53 m.

The palaeodata reconstruction errors are not defined. We conservatively treat the DP16 range as a mean ± 1 s.d. interval, so use σ_{obs} = {5, 2}m for the Pliocene and LIG respectively. The observational constraint (Shepherd et al., 2018)[25] is the cumulative mass loss from 1992-2017, (2720 ± 1390) Gt, converted to cm sea-level equivalent by dividing by 3600, to give (0.756 ± 0.386) cm sea-level contribution over this period. Model discrepancy is set to σ_{md} = 0.5 cm for 1992-2017 sea-level change.

When calibrating with palaeodata, we accept ensemble members with $I < 1$ for the Pliocene and LIG, so that the simplest case without emulator and model errors matches the interval used by DP16. We note this Pliocene range approximately corresponds to a 95% interval in some reconstructions, but the LIG range may correspond to a lower probability than 95% by some estimates, and so may be too strict a constraint (see main text). Calibration with satellite data observations accepts ensemble members with $I < 3$, to follow the usual history matching convention for well-defined errors: for a smooth unimodal distribution, $I < 3$ with probability greater than or equal to 95% (Pukelsheim, 1994)[36]'; for Gaussian distributions, as we expect for the satellite data errors, the probability interval is 99.7%.

Extended Data Figure 3 shows the 'calibration relationships' for RCP8.5 at 2100: the relationships between past and future. Grey boxes show the original palaeodata constraints; dashed lines show the broader intervals after accounting for model discrepancy. Accounting for emulator error in the implausibility means that some emulator ensemble members are accepted that lie just outside the calibration interval.

Percentiles and exceedance probabilities are estimated directly from the 10,000-member emulator ensemble, and modes from kernel density estimation using an automatic (Silverman) bandwidth. We do not include emulator uncertainties in the distributions; these are small at 2100, but increase on multi-century timescales so would broaden these distributions. To improve the clarity of Figure 3, we exclude 1, 3 and 5 data points from each of RCP8.5, RCP4.5 and RCP2.6 MICI projections respectively, because the estimates are not continuous in time (due to slight differences in emulator fitting).

Multi-model comparisons

We show distributions from Ruckert et al. (2016)[5] provided by Kelsey Ruckert, and estimate the distribution at 2100 for Little et al. (2013)[2] by digitisation of the original figures. We re-estimate the modes for Ritz et al. (2015)[4] distributions using an automatic bandwidth for the kernel density estimation, rather than the broader, fixed bandwidth used in the original study. We assume differences due to definitions of time period are small enough to be ignored: all are 2000-2100, except Little et al. (2013)[2] (1990-2099) and the IPCC[1] (1986–2005 to 2081–2100 for Antarctic component).

Palaeodata uncertainties

We here consider probability intervals for palaeodata constraints. Peak total sea-level change for the LIG estimated by Kopp et al. (2013)[39] is 6.4-10.9 m (90% probability interval), and by Dusterhus et al. (2016)[40] is 6.1-16.7m (80% probability). These broadly encompass recent

768 assessments that the upper end of the widely used 6-9 m range[49] could increase by several
769 metres[41]. Subtracting a range of estimates for the contributions from Greenland, thermal
770 expansion and glaciers in the same way as Ruckert et al. (2016)[5] (3.4-4.8 m) gives Antarctic
771 contributions of 1.6-7.5 m and 1.3-13.3 m respectively.
772 For the Pliocene, Miller et al. (2012)[37] estimate 22±10 m (95% range) total sea-level
773 change; subtracting 7 m for the Greenland ice sheet and 1 m for thermal expansion (Golledge
774 et al., 2017)[35] would imply approximately 14 ± 10 m Antarctic contribution, i.e. 4-24 m.
775 There is no difference between using a combined 5-25 m range and using the LowPliocene
776 (5-15 m) constraint presented here, because the DP16 ensemble maximum is 12.4 m, though
777 for a different model or ensemble design the upper bound might have more influence.
778 Golledge et al. (2017)[35] estimate 8.6 ± 2.8 m for the Antarctic contribution to the early
779 Pliocene, and we use their Gaussian assumption to derive the 95% (2σ) range.
780
781 **Code availability**
782 All emulation was performed in R using the DiceKriging and DiceEvaluation packages with
783 minor modifications by TLE. The scripts and input data for the main analysis (sea-level
784 projections at 2100) are available as a downloadable R package on GitHub
785 (https://github.com/tamsinedwards/revisitmici, v1.0.2) and can be run without installation on
786 the cloud-based computational reproducibility platform Code Ocean at
787 https://doi.org/10.24433/CO.4ebd8cda-35c0-4d8f-9b7c-d1b064109437.
788
789 **Data availability**
790 All projections from this study are available on request. Simulations of the LIG and Pliocene,
791 1992-2017 mean and 2100 sea level change for all DP16 ensemble members are available in
792 the Code Ocean data folder at the above link. Simulations at 2500 for the subset of the DP16
793 ensemble passing their calibration are available also in the Supplementary Materials of
794 DeConto and Pollard (2016).
795

796 Methods References

797

798 46. O'Hagan, A. Bayesian analysis of computer code outputs: A tutorial. *Reliability*
799 *Engineering and System Safety* 91, 1290–1300 (2006).
800 47. Sweet, W. V. *et al.* GLOBAL AND REGIONAL SEA-LEVEL RISE
801 SCENARIOS FOR THE UNITED STATES. 1–75 (2017).
802 48. Williamson, D. *et al.* History matching for exploring and reducing climate model
803 parameter space using observations and a large perturbed physics ensemble.
804 *Climate Dynamics* 41, 1703–1729 (2013).

49. Dutton, A. *et al.* Sea-level rise due to polar ice-sheet mass loss during past warm periods. *Science* 349, aaa4019–aaa4019 (2015).
50. Vernon, I., Goldstein, M. & Bower, R. G. Galaxy Formation: a Bayesian Uncertainty Analysis. *Bayesian Analysis* 5, 619–669 (2010).

Extended Data

Extended Data Figure 1. Sensitivity of DeConto and Pollard RCP8.5 projections to Pliocene data lower bound. DeConto and Pollard (2016) BiasUncorrected (a) and BiasCorrected (b) projections for Antarctic sea-level contribution by 2100 under RCP8.5 as a function of the lower bound of the Pliocene data range. Mean ± 1 s.d. range shown as central solid line with pink shading; mean ± 2 s.d. range as dotted line. (c) Sensitivity of emulated projections for RCP8.5 at 2100 with MICI from this study: [5, 25, 50, 75, 95]th percentiles and mode (*). Data from ref. 6.

Extended Data Figure 2. DeConto and Pollard RCP8.5 projection distributions. DeConto and Pollard (2016) ensemble projections for Antarctic sea-level contribution by 2100 under RCP8.5 for their four variants, LowPliocene BiasUncorrected (a) and BiasCorrected (b), and High Pliocene similarly (c, d), showing the full 64-member ensemble and the subset selected by calibrating with Pliocene and Last Interglacial sea-level reconstructions. The mean ± 1 s.d. range of the ensemble is shown as a solid red line with pink shading, and the 68% or greater probability interval is shown as a horizontal black line (see main text and Methods for more details). Data from ref. 6.

Extended Data Figure 3. Relationships between RCP8.5 projections at 2100 and past sea-level changes. Sea-level contribution at 2100 under RCP8.5 versus (a) Pliocene sea-level change; (b) Last Interglacial sea-level change; (c) sea-level change from 1992-2017, for the emulator (small grey dots) and DP16 simulator (large open circles) with ocean bias correction off (blue) and on (red). Grey shading indicates the DP16 palaeodata range (a, b) or observational mean ± 3 s.d. (c); the dashed line additionally includes model error. Data from refs. 6 and 25 and supplementary simulations by R. DeConto (pers. comm.) (see Methods).

Extended Data Figure 4. Relationship between past and future sea-level changes with and without MICI. Simulator ensemble (large circles), and emulated ensembles (small circles) with (a) cliff instability and (b) no cliff instability, showing Pliocene versus Last Interglacial sea-level changes and shaded by sea-level contribution at 2100 under RCP8.5. Large emulator points and filled simulator points pass the 1992-2017 calibration. Shaded rectangle indicates bounds of DP16 LowPliocene and Last Interglacial palaeodata constraints; dashed box shows constraints in this study, i.e. including model error. Data from refs. 6 and 25 and supplementary simulations by R. DeConto (pers. comm.) (see Methods).

Extended Data Figure 5. Sensitivity of RCP8.5 projections to MICI and calibration choices. Projections for RCP8.5 at 2100, with and without MICI, for different combinations of calibration eras ('palaeo': Pliocene and Last Interglacial; present: 1992-2017) and model discrepancy (with, without, and double). Box and whiskers show the [5, 25, 50, 75, 95]th percentiles; star shows the mode. Numbers show the median, [5th, 95th] percentiles and mode (*). Data from refs. 6 and 25 and supplementary simulations by R. DeConto (pers. comm.) (see Methods).

Extended Data Figure 6. Emulator validation. Left column: Emulator prediction versus simulation for each ensemble member, with the emulator fitted to the other ensemble members, for each of the outputs used for

building and validating emulator structure: RCP8.5, RCP4.5, and RCP2.6 sea-level contribution at 2100; 1992-2017 contribution; Last Interglacial; and Pliocene. Vertical error bars show 95% credibility intervals. Right column: Difference between emulator predictions and simulations, standardised by emulator error, for the same six outputs. Values falling mostly between ±2 indicate the emulator has adequate uncertainty estimates. Data from ref. 6 and supplementary simulations by R. DeConto (pers. comm.) (see Methods).

Extended Data Figure 7. Sensitivity of RCP8.5 projections to model parameters. Sea-level contribution at 2100 under RCP8.5 versus VCLIF (a), CREVLIQ (b) and OCFAC (c) parameters for emulator (small grey dots with error bars) and simulator (large open circles: BiasUncorrected blue, BiasCorrected red). Data from ref. 6 and supplementary simulations by R. DeConto (pers. comm.) (see Methods).

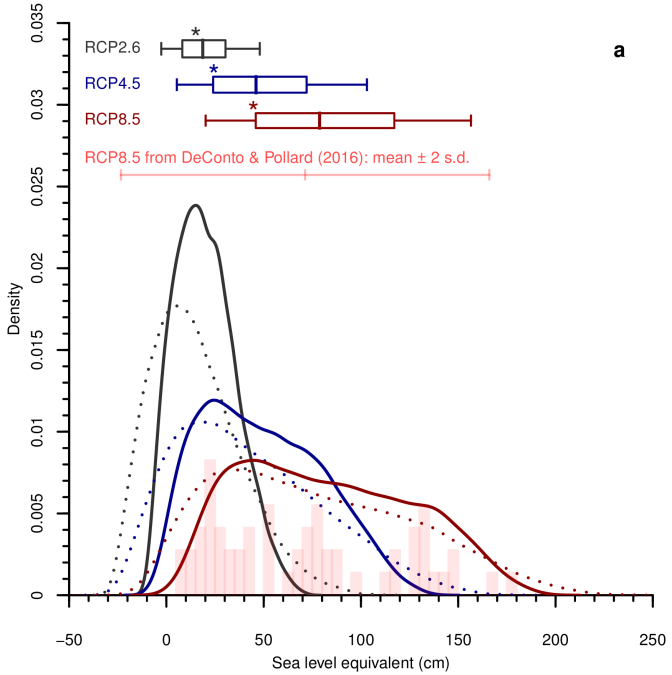
a
RCP2.6
RCP4.5
RCP8.5
RCP8.5 from DeConto & Pollard (2016): mean ± 2 s.d.
Density
0
0.005
0.01
0.015
0.02
0.025
0.03
0.035
−50
0
50
100
150
200
250
Sea level equivalent (cm)

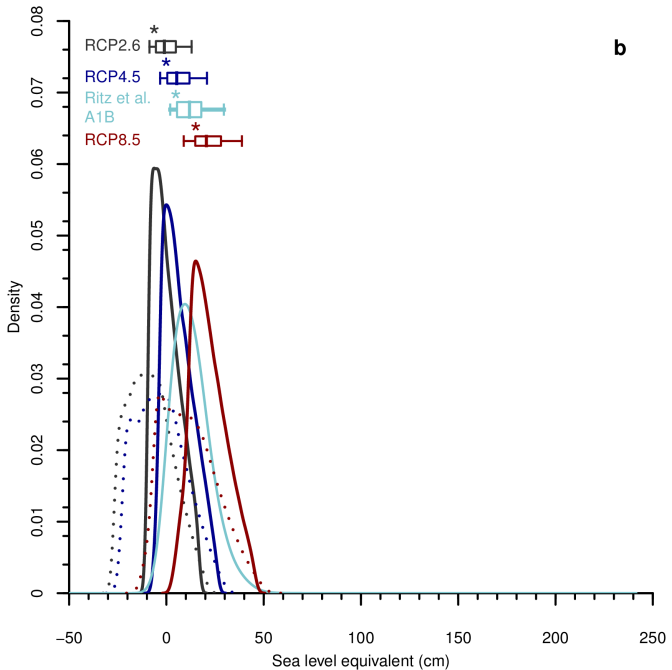
b
RCP2.6
RCP4.5
Ritz et al.
A1B
RCP8.5
Density
0
0.01
0.02
0.03
0.04
0.05
0.06
0.07
0.08
−50
0
50
100
150
200
250
Sea level equivalent (cm)

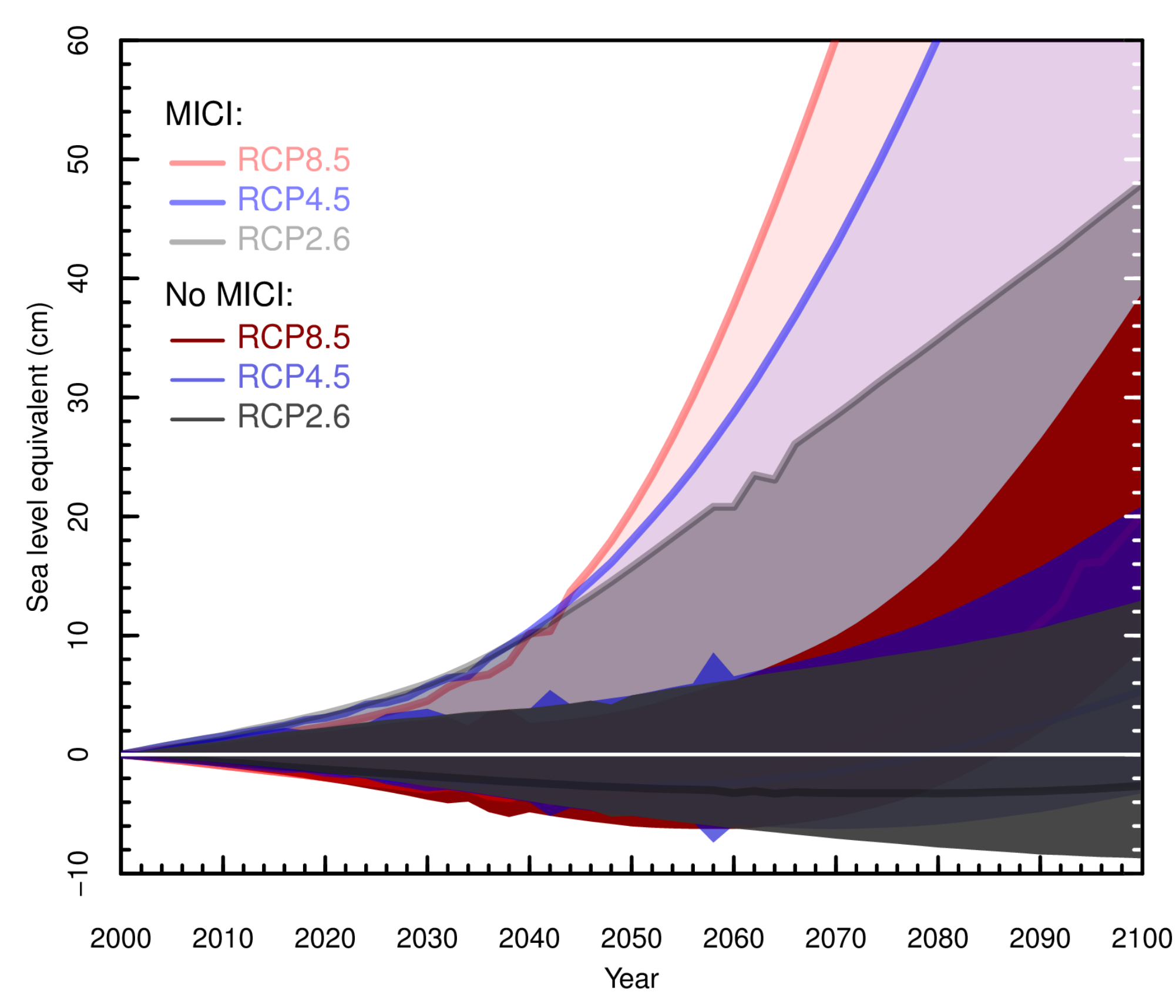
MICI:
RCP8.5
RCP4.5
RCP2.6
No MICI:
RCP8.5
RCP4.5
RCP2.6
Sea level equivalent (cm)
60
50
40
30
20
10
0
−10
2000
2010
2020
2030
2040
2050
2060
2070
2080
2090
2100
Year

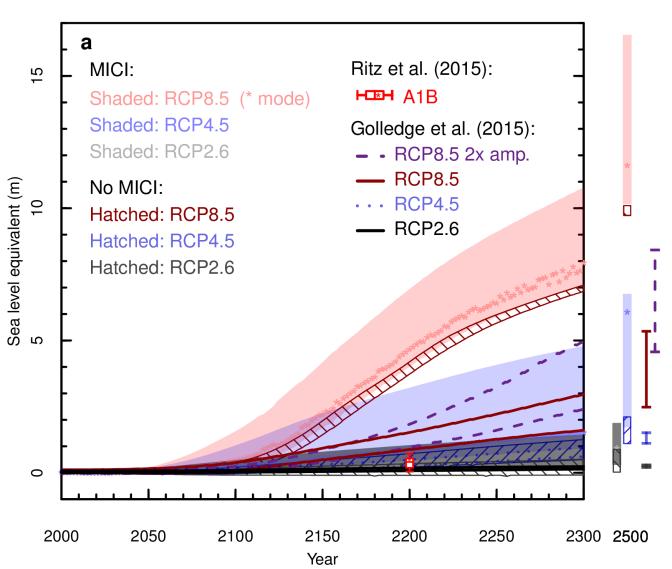
a
MICI:
Shaded: RCP8.5 (* mode)
Shaded: RCP4.5
Shaded: RCP2.6
No MICI:
Hatched: RCP8.5
Hatched: RCP4.5
Hatched: RCP2.6
Ritz et al. (2015):
A1B
Golledge et al. (2015):
RCP8.5 2x amp.
RCP8.5
RCP4.5
RCP2.6
Sea level equivalent (m)
0
5
10
15
2000
2050
2100
2150
2200
2250
2300
2500
Year

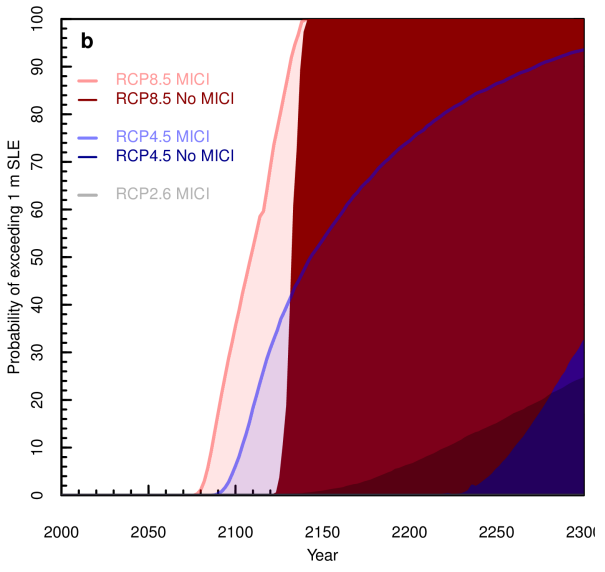
b
RCP8.5 MICI
RCP8.5 No MICI
RCP4.5 MICI
RCP4.5 No MICI
RCP2.6 MICI
Probability of exceeding 1 m SLE
0
10
20
30
40
50
60
70
80
90
100
2000
2050
2100
2150
2200
2250
230
Year

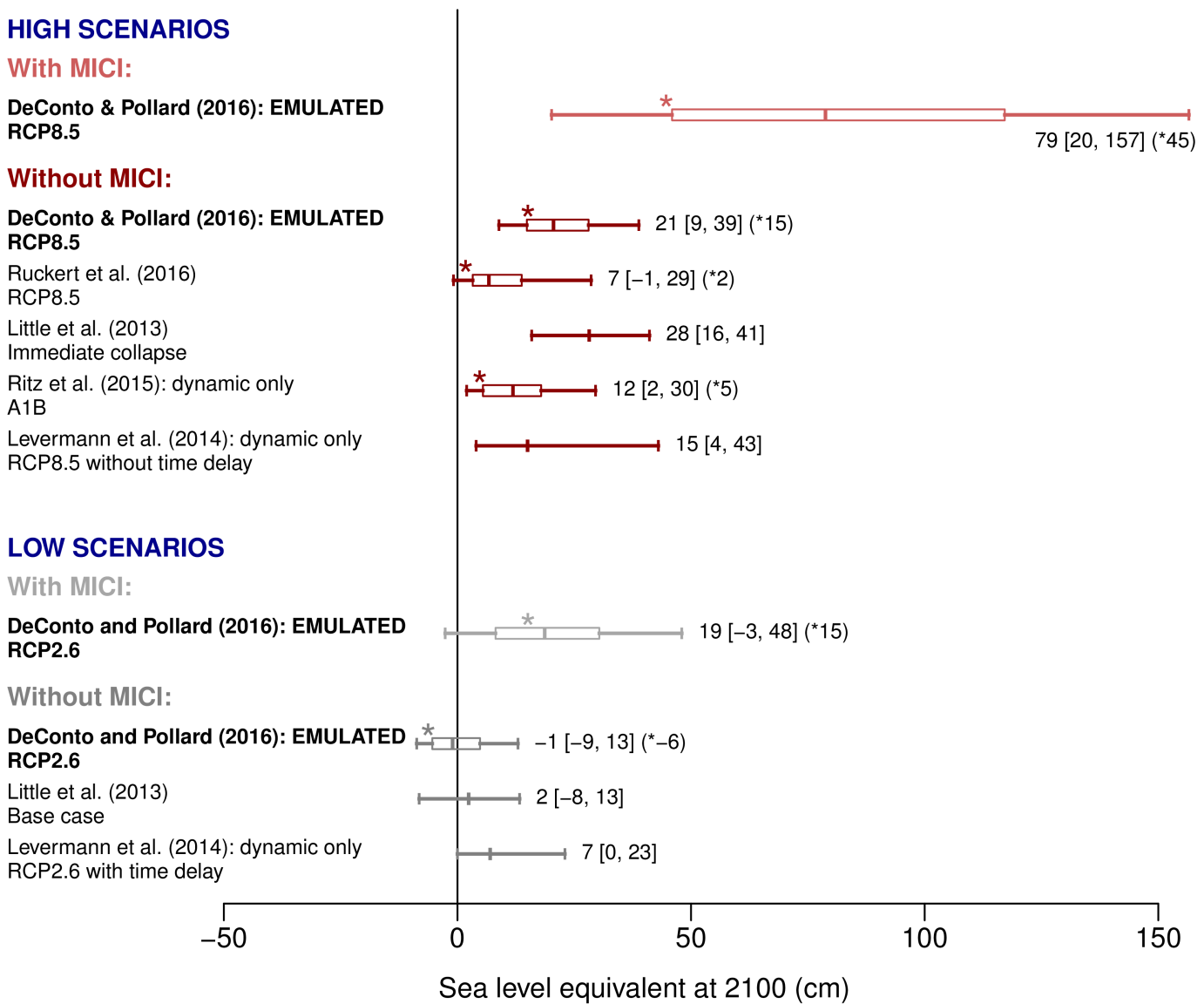
HIGH SCENARIOS
With MICI:
DeConto & Pollard (2016): EMULATED
RCP8.5
79 [20, 157] (*45)
Without MICI:
DeConto & Pollard (2016): EMULATED
RCP8.5
21 [9, 39] (*15)
Ruckert et al. (2016)
RCP8.5
7 [−1, 29] (*2)
Little et al. (2013)
Immediate collapse
28 [16, 41]
Ritz et al. (2015): dynamic only
A1B
12 [2, 30] (*5)
Levermann et al. (2014): dynamic only
RCP8.5 without time delay
15 [4, 43]
LOW SCENARIOS
With MICI:
DeConto and Pollard (2016): EMULATED
RCP2.6
19 [−3, 48] (*15)
Without MICI:
DeConto and Pollard (2016): EMULATED
RCP2.6
−1 [−9, 13] (*−6)
Little et al. (2013)
Base case
2 [−8, 13]
Levermann et al. (2014): dynamic only
RCP2.6 with time delay
7 [0, 23]
−50
0
50
100
150
Sea level equivalent at 2100 (cm)

a

b

c

Mean and std dev SLE for RCP8.5 at 2100 (cm)

Mode and quantiles SLE for RCP8.5 at 2100 (cm)

-50 0 50 100 150 200 250

0 1 2 3 4 5 6 7 8 9 10 11

Lower bound Pliocene (m SLE)

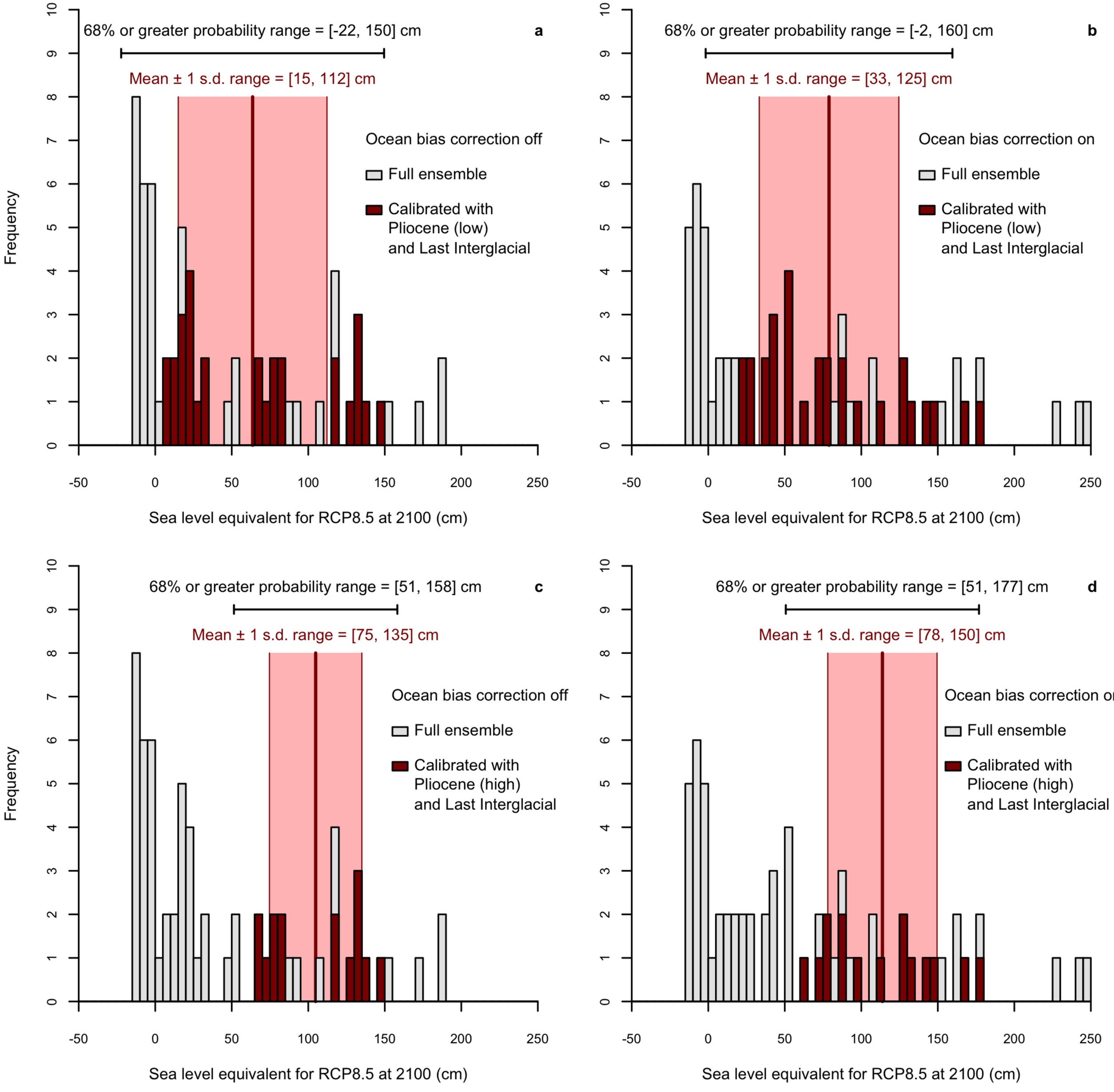
a
68% or greater probability range = [-22, 150] cm
Mean ± 1 s.d. range = [15, 112] cm
Ocean bias correction off
Full ensemble
Calibrated with Pliocene (low) and Last Interglacial
b
68% or greater probability range = [-2, 160] cm
Mean ± 1 s.d. range = [33, 125] cm
Ocean bias correction on
Full ensemble
Calibrated with Pliocene (low) and Last Interglacial
c
68% or greater probability range = [51, 158] cm
Mean ± 1 s.d. range = [75, 135] cm
Ocean bias correction off
Full ensemble
Calibrated with Pliocene (high) and Last Interglacial
d
68% or greater probability range = [51, 177] cm
Mean ± 1 s.d. range = [78, 150] cm
Ocean bias correction on
Full ensemble
Calibrated with Pliocene (high) and Last Interglacial
Frequency
0
1
2
3
4
5
6
7
8
9
10
-50
0
50
100
150
200
250
Sea level equivalent for RCP8.5 at 2100 (cm)

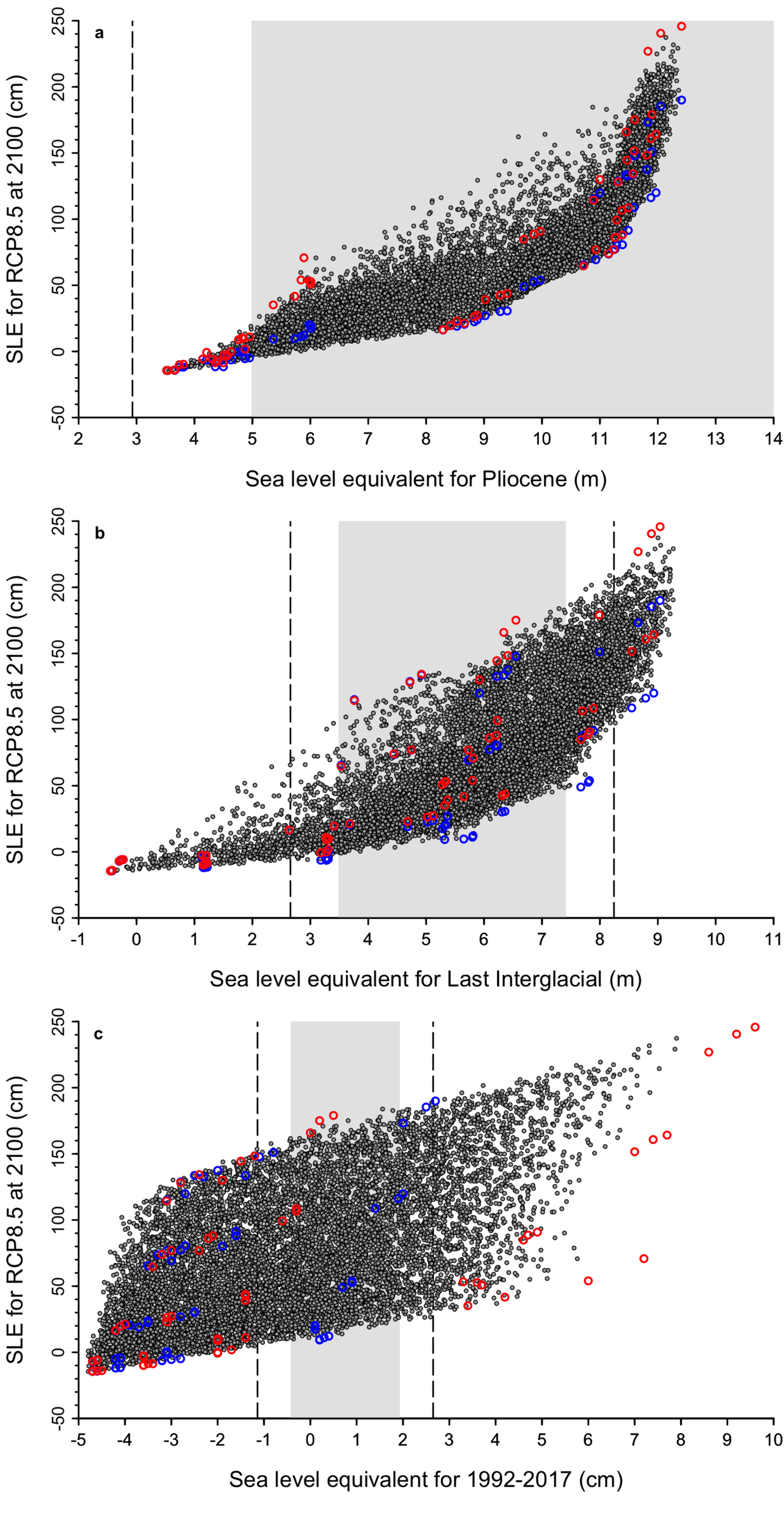
a
SLE for RCP8.5 at 2100 (cm)
Sea level equivalent for Pliocene (m)
b
SLE for RCP8.5 at 2100 (cm)
Sea level equivalent for Last Interglacial (m)
c
SLE for RCP8.5 at 2100 (cm)
Sea level equivalent for 1992-2017 (cm)

a

Sea level equivalent for Pliocene (m)

Sea level equivalent for Last Interglacial (m)

SLE for RCP8.5 at 2100 (cm)

250.0
200.0
150.0
100.0
50.0
0.0
-50.0

b

Sea level equivalent for Pliocene (m)

Sea level equivalent for Last Interglacial (m)

SLE for RCP8.5 at 2100 (cm)

250.0
200.0
150.0
100.0
50.0
0.0
-50.0

MICI:

Palaeo & present

79 [20, 157] (*45)

Palaeo only

69 [12, 156] (*37)

Present only

81 [20, 159] (*45)

Palaeo & present;
double discrepancy

78 [15, 161] (*44)

Palaeo & present;
no discrepancy

70 [21, 150] (*43)

Palaeo;
no discrepancy

64 [15, 141] (*41)

Palaeo & present;
VCLIF <= 4 km/a

68 [19, 131] (*41)

No-MICI:

Palaeo & present

21 [9, 39] (*15)

Palaeo only

15 [1, 39] (*9)

Present only

21 [9, 39] (*15)

Palaeo & present;
double discrepancy

17 [4, 39] (*9)

Palaeo & present;
no discrepancy

23 [13, 38] (*18)

Palaeo;
no discrepancy

20 [7, 41] (*16)

-50 0 50 100 150

Sea level equivalent at 2100 (cm)

RCP8.5 at 2100 (cm)

RCP4.5 at 2100 (cm)

RCP2.6 at 2100 (cm)

1992-2017 (cm)

Last Interglacial (m)

Pliocene (m)

Emulated sea level equivalent (units in label)

Simulated sea level equivalent (units in label)

Standardised residuals

Frequency

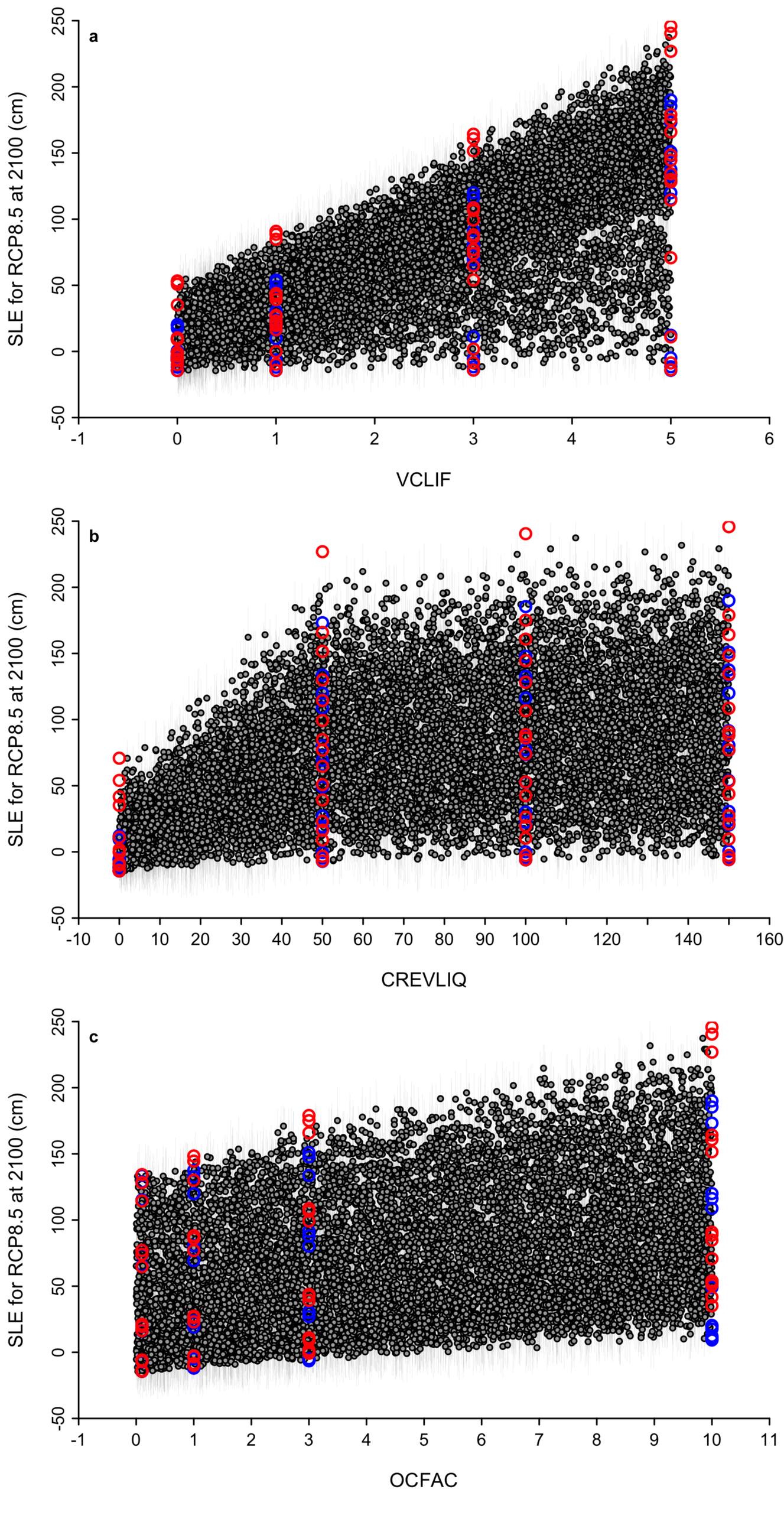
a
SLE for RCP8.5 at 2100 (cm)
250
200
150
100
50
0
-50
-1
0
1
2
3
4
5
6
VCLIF
b
SLE for RCP8.5 at 2100 (cm)
250
200
150
100
50
0
-50
-10
0
10
20
30
40
50
60
70
80
90
100
120
140
160
CREVLIQ
c
SLE for RCP8.5 at 2100 (cm)
250
200
150
100
50
0
-50
-1
0
1
2
3
4
5
6
7
8
9
10
11
OCFAC